ADVANCED FUNCTIONAL MATERIALS
www.afm-journal.de

Two-Photon Pumped Single-Mode Lasing in $CsPbBr_3$ Perovskite Microwire

Junfeng Lu, Xiaopeng He, Juan Xu, Fangtao Li, Qingbin Tang,* Xiaoxuan Wang, Jun Dai, Qiushi Yao, Feifei Qin, and Chunxiang Xu**

Achieving high-quality, frequency-upconversion single-mode lasing output is an important requirement for developing new nonlinear optoelectronic devices, such as on-chip optical communication, nonlinear optical switches, and optical parametric amplifiers. Here, an individual $CsPbBr_3$ microwire prepared by the anti-solvent method is served as both gain media and microresonator to achieve two-photon pumped frequency upconversion single-mode lasing with the side-mode suppression ratio of 18 dB. Meanwhile, the refractive index of orthorhombic perovskite is theoretically calculated based on first principles, and determining its square whispering-gallery oscillation type by combining with the plane wave model and the steady-state oscillation conditions of laser. The extracted exciton binding energy of 33.15 meV higher than the thermal ionization energy of room temperature (≈26 meV) suggests that the as-grown $CsPbBr_3$ microwires possess the capacity to achieve two-photon pumped lasing output, as well further gaining deeper insights into the role of exciton-phonon coupling in light emission.

1. Introduction

Halide perovskite materials have attracted extensive attention in the field of optoelectronic devices such as light-emitting diodes,[1–3] photodetectors,[4–6] and solar cells,[7–9] due to their advantages of high fluorescence quantum efficiency, wide wavelength tunable range, high optical absorption coefficient, long carrier lifetime and diffusion length.[10–12] Besides, the flexible and diverse preparation methods of perovskite micro nanocrystals provide convenient conditions for designing different resonant cavities,[13–15] to meet various needs. Typically, perovskite nanowires and microplates can serve as natural microcavities for Fabry-Pérot (FP) and whispering-gallery mode (WGM) oscillation types, as well as providing sufficient gain for optical amplification. In particular, a significant amount of milestone works on single-photon pumped high-quality, low threshold lasers has been reported,[16–18] based on all-inorganic perovskite materials $CsPbX_3$ (X = Cl, Br, I) thanks to their excellent chemical stability. Recently, the multiphoton absorption (MPA) involving simultaneous absorption of multiple monochromatic lower energy photons to excite an electron transition to a higher energy state and subsequently relaxing to yield the emission of a higher energy photon have found widespread applications in 3D biomedical imaging,[19,20] frequency upconversion lasers,[21,22] optical power limitation.[23] However, the nonlinear optical processes have strict demands on optical properties of the gain medium, such as large optical gain and high cross section of MPA. Among the available candidate materials, all-inorganic low-dimensional perovskite has emerged as the focus on nonlinear absorption and emission,[24–26] because of their near 100% fluorescence quantum efficiency and the large

J. Lu, X. He, J. Xu, Q. Yao
College of Physics
Nanjing University of Aeronautics and Astronautics
Nanjing 211106, P. R. China
E-mail: lujunfeng@nuaa.edu.cn
J. Lu, X. He, J. Xu, Q. Yao
Key Laboratory of Aerospace Information Materials and Physics (NUAA) MIIT
Nanjing 211106, P. R. China
F. Li, Q. Tang
School of Physics and Electronic Engineering
Xinyang Normal University
Xinyang 464000, P. R. China
E-mail: qingbintang@xynu.edu.cn
X. Wang, C. Xu
State Key Laboratory of Bioelectronics
School of Biological Science and Medical Engineering
Southeast University
Nanjing 210096, P. R. China
E-mail: xcxseu@seu.edu.cn
J. Dai
College of Science
Jiangsu University of Science and Technology
Zhenjiang 212100, P. R. China
F. Qin
Peter Grünberg Research Centre
Nanjing University of Posts and Telecommunications
Nanjing 210003, P. R. China

The ORCID identification number(s) for the author(s) of this article can be found under https://doi.org/10.1002/adfm.202308957

DOI: 10.1002/adfm.202308957

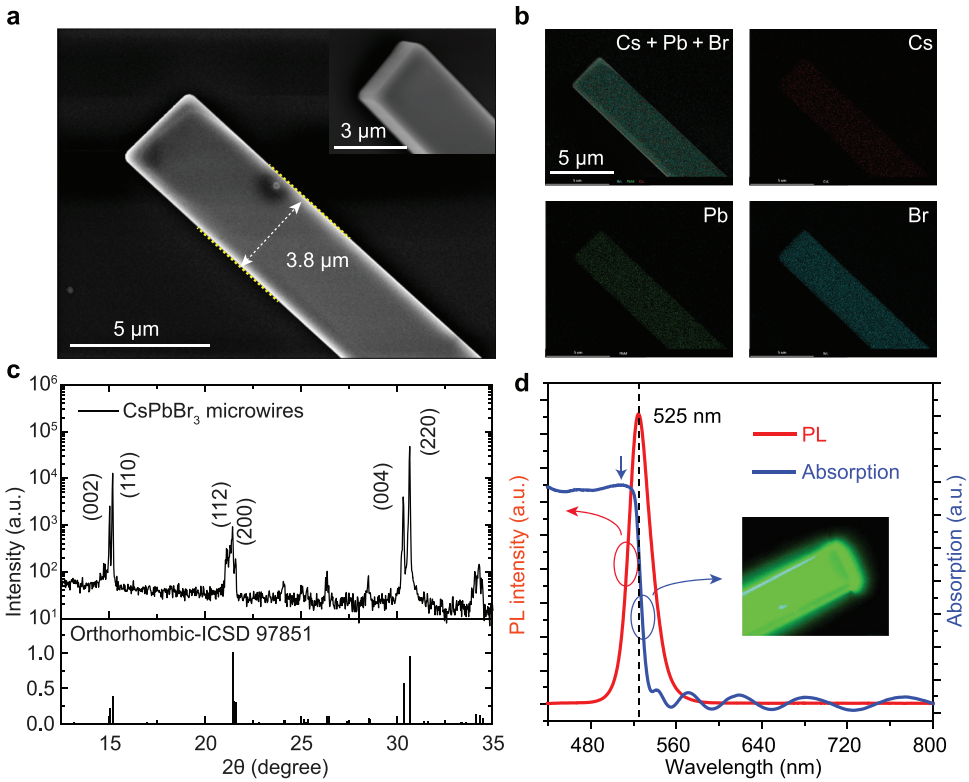

Figure 1. Morphological, structural, and optical characterization. a) SEM image of $CsPbBr_3$ perovskite microwires, illustrated with an inclination angle view; b) EDS mapping of Cs, Pb, Br elements; c) X-ray diffraction (XRD) patterns and standard card (ICSD 97851) of $CsPbBr_3$ microwires with the orthorhombic phase; d) the steady-state photoluminescence and absorption spectra of single perovskite microwire inserted with an image of PL imaging.

two-photon-absorption cross-section of 2.7×10^6 GM.[27] Meanwhile, the large exciton binding energy (50 meV) exceeding the thermal ionization energy of room temperature (26 meV) endows the necessary conditions for constructing perovskite-based frequency up-conversion lasers, making it easier to achieve population inversion of particles. Moreover, this multiphoton-pumping mechanism with low photon energy exhibits many attractive merits over linear excitation, such as high spatial localization, long penetration depth, and low damage effect.

Herein, the anti-solvent method has been utilized to prepare $CsPbBr_3$ microwires with a square cross-section, which can serve as both optical microresonators and gain medium. Combined with the intrinsic self-absorption effect of perovskite,[18] the two-photon pumped frequency upconversion single-mode lasing output with a Q factor of 3200 is realized in an individual $CsPbBr_3$ microwire with the width of 2 μm. Moreover, the dispersion relation of the refractive index of orthorhombic-phase $CsPbBr_3$ versus the incident photon energy is calculated by the first-principles based on density functional theory. Then, the expression of mode number for the square WGM microcavity is further derived according to the plane wave model and the laser steady-state oscillation conditions. The estimated resonant wavelengths are in good agreement with the experimental values, which fundamentally clarifies the attribution of the oscillation type of light waves in the cross-section of $CsPbBr_3$ microwire.

2. Results and Discussion

Figure 1a demonstrates a typical scanning electron microscope (SEM) top and tilt views of the selected single $CsPbBr_3$ microwire with a width of 3.8 μm. The smooth surface and rectangular cross-section of perovskite microwire indicate that it is a natural resonant cavity, where the light waves can be fully confined and totally reflected at the four inner walls to form the whispering-gallery oscillation type. The energy dispersive spectroscopy (EDS) mapping of Cs, Pb, and Br elements shown in Figure 1b indicates that the distribution of each composition in the prepared perovskite microwire is uniform. Meanwhile, its structure is characterized by X-ray diffraction (XRD) as shown in Figure 1c, which suggests that the prepared $CsPbBr_3$ microwires belong to the orthorhombic phase (space group *Pbnm*). The six obvious diffraction peaks shown in the XRD pattern located at 15.03°, 15.19°, 21.44°, 21.62°, 30.35°, and 30.68°, can be assigned to the (002), (110), (112), (200), (004), and (220) crystal planes, respectively, in agreement with the ICSD 97851 of $CsPbBr_3$. In addition, the typical diffraction peak splitting at around 15° and 30° further verified the room-temperature orthorhombic phase structure of the prepared $CsPbBr_3$ perovskite microwires. Also, the fluorescence imaging, steady-state photoluminescence (PL), and absorption spectra of single perovskite microwire are measured, as shown in Figure 1d. A strong spontaneous emission peak at 525 nm corresponding to the absorption band edge can be observed, indicating that it

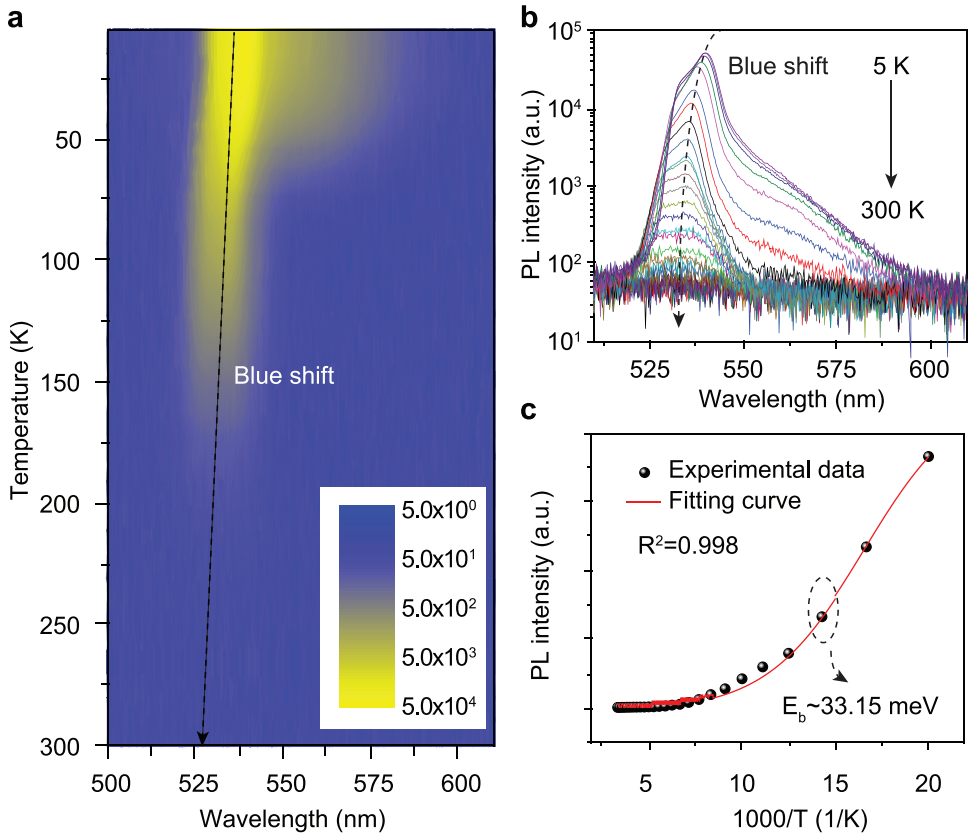

Figure 2. Temperature-dependent PL spectra. a) 2D pseudo-color plots and b) spectral profiles of PL spectra for $CsPbBr_3$ microwires at different temperatures ranging from 5 to 300 K; c) the dependence of PL intensity on temperature.

originates from the intrinsic radiation recombination between electrons from conduction band and holes from valence band. The dazzling and uniform green light emission (see Figure S1, Supporting Information) further indicates that individual $CsPbBr_3$ microwire is not only a natural resonant cavity, but also provides sufficient gain for light amplification. It is worth noting that a weak exciton absorption peak can be observed near the absorption band edge at room temperature, which is associated with bound excitonic states in the materials.

In order to gain more insights into the role of phonons in the intrinsic radiation recombination of perovskite, temperature-dependent PL spectra measurements were performed at the temperature ranging from 5 K to 300 K. **Figure 2**a shows the 2D pseudo color mapping of temperature-dependent PL for $CsPbBr_3$ microwires, and the corresponding PL spectra are demonstrated in Figure 2b. As the temperature increases, the central wavelength of PL emission peak exhibits a continuous blue shift phenomenon from 539.9 to 525.6 nm, accompanied by the full width at half maximum (FWHM) broadening, which can be attributed to thermal expansion and electron-phonon interaction.[28,29] The nearly linear relationship in the low-temperature range is mainly dominated by thermal expansion (see Figure S3c, Supporting Information), whose tendency is opposite to that of conventional semiconductors. This is because the lattice dilation at higher temperatures reduces the hybridization between the 6s and 4p orbitals from Pb and Br that form valence band maxima, and leading to the widening of the band gap.[30] In the high-temperature region, the sub-linear relationship originates from the synergistic effect of thermal expansion and electron-phonon coupling, where the latter reduces the increased rate of band gap caused by thermal expansion.[31] It is worth noting that the PL spectra of $CsPbBr_3$ microwires exhibit slight asymmetry at a temperature as low as 190 K, which arises from the appearance of the weak peak (P2) emission on the low energy side of the band-edge peak (P1). As the temperature further decreases, the intensity of side-peak emission sharply increases and dominates at 150 K (see Figure S3, Supporting Information). To explore the causes of the side peak, the operating temperature of PL spectra is further reduced. As the temperature drops below 70 K, another emission peak (P3) appears on the low energy side of P2, where the PL spectra exhibit distinct asymmetry. Gaussian fitting was performed on the asymmetric PL spectrum at 5 K, and three peaks located at 2.3208 eV (blue dashed line), 2.2965 eV (green dashed line), and 2.2722 eV (red dashed line) are observed (see Figure S3, Supporting Information) in this case. Both of the energy spacing is 24.3 meV, which is similar to the longitudinal optical (LO) phonon energy of ≈20 meV for the bulk and nanosized $CsPbBr_3$ samples.[32,33] Therefore, P2 and P3 can be attributed to the first-order phonon replicas (FX-1LO) and second-order phonon replicas (FX-2LO) of the free-exciton (FX) principal zero phonon line (ZPL), respectively, revealing the role of exciton-phonon coupling in light emission of $CsPbBr_3$ microwires. In addition, another

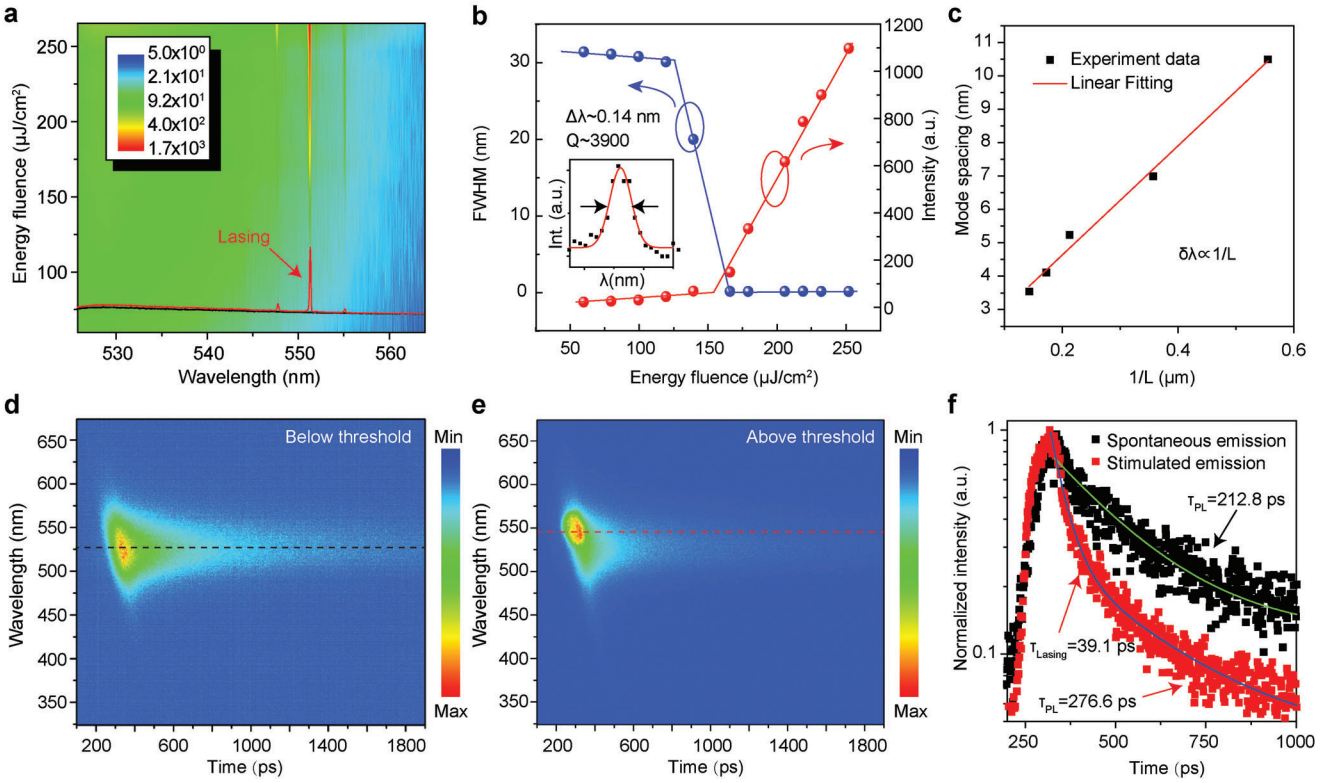

Figure 3. Lasing characteristics and luminescent dynamics. a) 2D pseudo-color plots of lasing spectra for single $CsPbBr_3$ microwire at different pumping energy fluences; b) the dependence of emission intensity and FWHM on energy fluences; c) mode spacing as a function of the reciprocal of cavity length (L); temporal spectroscopic profiles of single $CsPbBr_3$ microwire d) below and e) above the lasing threshold (P_{th}) collected by a streak camera; f) time-resolved photoluminescence (TRPL) of spontaneous and stimulated emission.

important characteristic of temperature-dependent PL spectra is the dramatically decreasing of emission intensity with the increasing of temperature, which can be attributable to the thermally activated non-radiative recombination process,[34] Figure 2c shows the dependence of PL emission intensity on temperature, which can be fitted by the Arrhenius equation of $I\,(T) = I_0/(1 + Ae^{-E_b/k_bT})$, where I_0 represents the PL emission intensity at 0 K, A is the proportional coefficient, E_b is the exciton binding energy, and k_b is the Boltzmann constant. In this case, the exciton binding energy E_b is extracted as 33.15 meV through fitting, which is higher than the thermal ionization energy of room temperature (≈26 meV). This suggests that excitons can still exist at room temperature, which corresponds to the weak exciton absorption peak observed in the absorption spectrum of Figure 1d. It is beneficial for achieving population inversion of particles and providing necessary conditions for building the lasers operating at room temperature.

Figure 3 demonstrates the single-photon lasing characteristics for individual 7 μm-wide and 155 μm-long $CsPbBr_3$ microwire pumped by a femtosecond laser with a wavelength of 355 nm (see Figure S4, Supporting Information). The 2D pseudo-color plots of lasing spectra under different pumping energy fluences are shown in Figure 3a. As the pumping energy fluence increases and exceeds to 150 μJ cm^{-2}, the lasing spectrum evolves from the wide spontaneous emission to the stimulated emission with the extremely narrow FWHM, accompanied by a sharp increase in emission intensity shown in Figure 3b. The Q factor of lasing can be estimated as ≈3900 according to $Q = \lambda/\Delta\lambda$, indicating the excellent capacity of single crystal perovskite microresonator for the optical-field confinement because of its tetragonal configuration and large refractive index. The $CsPbBr_3$ dispersion relation for the orthogonal phase is calculated by using the first principle. The detailed methods can be seen in Figure S5, Supporting Information, where the dependence of its refractive index on the photon energy is described. Then, combined with the plane wave model and steady-state oscillation conditions, the formula for calculating the TE mode number (N) of the square whispering-gallery (WG) microcavity in this case is derived as $N = \frac{2\sqrt{2}nL}{\lambda} - \frac{4}{\pi}tan^{-1}(n\sqrt{n^2-2})$, where L is the length of the cavity, n is the refractive index, λ is the resonant wavelength. The mode numbers of the resonant wavelengths located at 547.87, 551.43, 555.27 nm for the microresonators with the cavity length of 7 μm are assigned as 113, 112, 111 (see Figure S6, Supporting Information), respectively. The experimental and calculated values of the resonant wavelength are in good agreement, proving the formation of the square WG oscillation model. As the cavity size gradually decreases, the mode spacing, also known as the free spectral range, will gradually increase (see Figure S7, Supporting Information). Figure 3c shows the dependence of mode spacing on the cavity size, which is proportional to the reciprocal of the latter. As the cavity size reduces to ≈2 μm, the single-mode lasing output is formed due to the existence of self-absorption effect and the enlarged mode spacing.[35,36] To investigate the

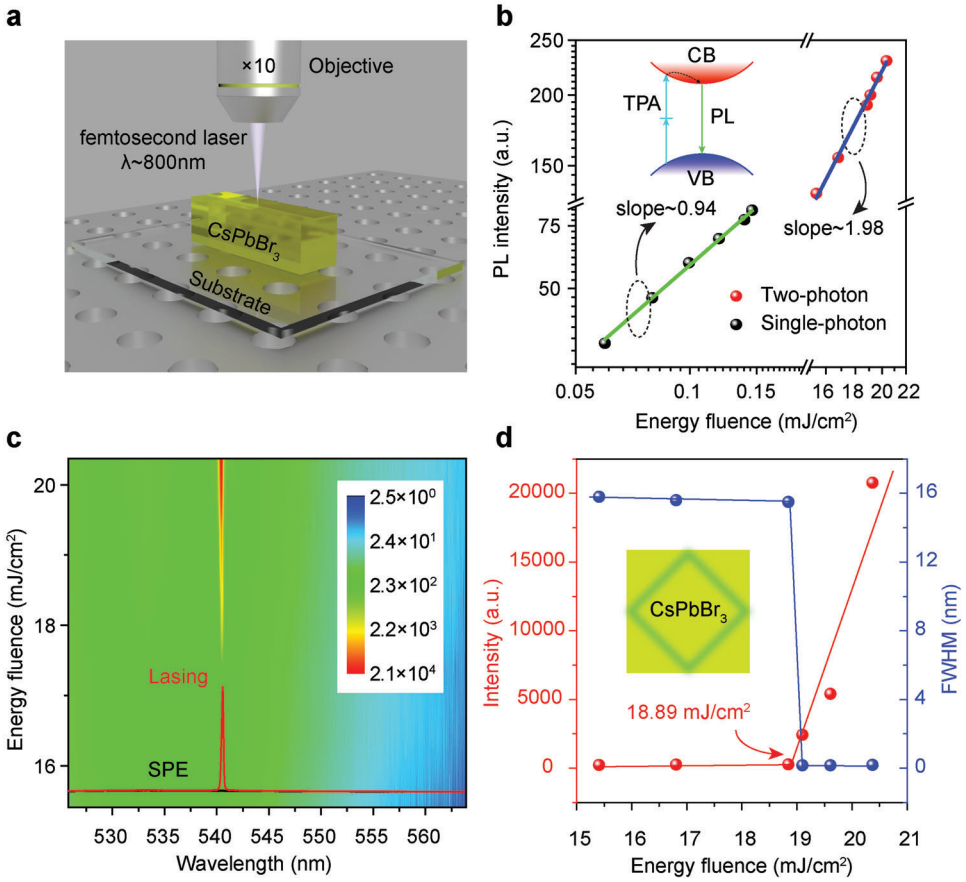

Figure 4. Two-photon pumped single-mode lasing. a) Schematic diagram of μ-PL system; b) the integrated PL intensity as a function on energy fluences at the excited wavelengths of 355 and 800 nm fitting by a power exponential function; c) 2D pseudo-color plots of two-photon pumped single-mode lasing spectra for single $CsPbBr_3$ perovskite microwire at different energy fluences; d) the dependence of emission intensity and FWHM on energy fluences.

dynamic lasing behavior of single $CsPbBr_3$ microcavity, the measurement of time-resolved PL spectroscopy is performed through a streak camera at room temperature. Figure 3d,e shows the temporal spectroscopic profiles when the pumping energy fluence (P_{in}) is below and above the lasing threshold (P_{th}), respectively. As P_{in} exceeds P_{th}, the typical stimulated emission with extremely narrow linewidth is observed on the low energy side of the spontaneous emission (see Figure S8, Supporting Information). The time-resolved PL spectra of the spontaneous and stimulated transition processes shown in Figure 3f demonstrate the decay tendency of emission intensity with time, which can be fitted by the monoexponential and biexponential functions, respectively. When P_{in} is less than P_{th}, a long decay time of ≈212.8 ps is obtained by the fitting of monoexponential function. As P_{in} exceeds P_{th}, an ultrafast decay component (≈39.1 ps) and a relatively slower process (≈276.6 ps) are observed by the fitting of biexponential function, further suggesting the transition from spontaneous emission to stimulated emission.[37]

Furthermore, two-photon pumped lasing characteristics of individual $CsPbBr_3$ perovskite microcavity with a width and length of 2 and 140 μm (see Figure S9, Supporting Information), respectively, are measured to reveal its nonlinear optical behavior using the same μ-PL system excited by a femtosecond laser with the wavelength of 800 nm, as shown in **Figure 4**a. Figure 4b compares the dependence of PL intensity and pumping energy fluences under single-photon and two-photon excitation at the wavelength of 355 and 800 nm, respectively, which can be fitted by the power exponential function of $I \propto p^{\gamma}$. The power-law exponents γ of both are ≈0.94 and ≈1.98, respectively, when exciting by 355 and 800 nm femtosecond lasers. The former presents an approximately linear relationship between PL intensity and pumping energy fluences, implying the dominated single-photon excitation process. Whereas, the latter demonstrates a quadratic power dependence, suggesting the participation of two-photon absorption process because of the lower excitation photon energy, as shown in the illustration of Figure 4b. When further increasing the pumping energy fluence, a sharp peak with the extremely narrow FWHM of ≈0.17 nm (see Figure S9, Supporting Information) appears at the low energy side of the intrinsic spontaneous emission, suggesting a transition to stimulated emission. Figure 4d plots the dependence of pumping energy fluence on emission intensity and FWHM with an estimated threshold of ≈18.89 mJ cm^{-2}, which is two orders of magnitude larger than single-photon lasing. This further confirms that the efficiency of the two-photon lasing process is much lower than that of the single-photon lasing process. However, the lasing Q factor has not been seriously affected and remains at about 3200; Meanwhile, the lasing output also exhibits single-mode characteristics,

and its side-mode suppression ratio (SMSR) can be estimated as 18.0 dB (see Figure S10, Supporting Information) by formula of SMSR = $10\log(M_1/M_2)$, where M_1 and M_2 are the intensity of the dominant mode and side mode. These results indicate that $CsPbBr_3$ perovskite microcrystals provide a natural configuration for constructing high-quality, frequency up-conversion single-mode lasers.

3. Conclusion

In summary, we have achieved high-quality two-photon pumped single-mode lasing output in individual $CsPbBr_3$ microwire with the Q-factor of 3200 and SMSR of 18 dB excited by 800 nm femtosecond laser. The measurement of temperature-dependent PL spectra is performed to elucidate the role of exciton-phonon coupling in perovskite light emission. Two emission peaks on the low energy side of the band-edge emission are assigned to the first-order phonon replicas (FX-1LO) and second-order phonon replicas (FX-2LO) respectively, revealing the physical roots of asymmetric PL spectra at cryogenic temperature. The estimated exciton binding energy of 33.15 meV is significantly larger than the thermal ionization energy of room temperature (≈26 meV), which is conducive to achieving particle population inversion. These results provide important scientific basis for constructing high-quality, frequency up-conversion single-mode lasers.

4. Experimental Section

The anti-solvent method was used to prepare $CsPbBr_3$ perovskite microwires with the length ranging from 50 to 200 µm and the width ranging from 1 to 20 µm (see Figure S1, Supporting Information), which is described specifically in the previous reports.[38,39] The morphology and elemental composition of microwires were characterized by field-emission scanning electron microscope equipped with EDS. The structure of the samples was measured by XRD. The PL spectrum, absorption spectrum, as well as PL mapping were measured by a highly integrated self-made micro-system, consisting of the spectrometer, microscope, and displacement stage. The temperature was controlled by a cryogenic system (Janis 150c), covering a range from 5 K to room temperature. The lasing performance of $CsPbBr_3$ microcavity was characterized by a μ-PL system (see Figure S2, Supporting Information) coupled with a wavelength-tunable femtosecond laser system (190 fs, 6000 Hz), an upright microscope (×10/×20/×40/×100), and an optical multi-channel spectrometer (300/600/1200 g mm^{-1}). The measurement of time-resolved PL spectra was performed by a streak camera (2 ps) equipped with an optical multi-channel spectrometer (150/600/1800 g mm^{-1}) and a femtosecond laser system (100 fs, 1000 Hz) with the excited wavelength of 325 nm.

Supporting Information

Supporting Information is available from the Wiley Online Library or from the author.

Acknowledgements

J. L., X. H., and J. X. contributed equally to this work. The authors thank the support of the Fundamental Research Funds for the Central Universities (no. NS2022096), the National Natural Science Foundation of China (nos. 61805015, 12374257), the Open Research Fund of State Key Laboratory of Bioelectronics, Southeast University (no. SKLB2022-P01), and the Postgraduate Research and Practice Innovation Project of Nanjing University of Aeronautics and Astronautics (no. xcxjh20222101).

Conflict of Interest

The authors declare no conflict of interest.

Data Availability Statement

The data that support the findings of this study are available from the corresponding author upon reasonable request.

Keywords

$CsPbBr_3$, laser, single-mode, two-photon absorption, whispering-gallery mode

Received: July 31, 2023
Revised: September 21, 2023
Published online: October 20, 2023

[1] Y. Cao, N. Wang, H. Tian, J. Guo, Y. Wei, H. Chen, Y. Miao, W. Zou, K. Pan, Y. He, H. Cao, Y. Ke, M. Xu, Y. Wang, M. Yang, K. Du, Z. Fu, D. Kong, D. Dai, Y. Jin, G. Li, H. Li, Q. Peng, J. Wang, W. Huang, *Nature* **2018**, *562*, 249.
[2] K. Lin, J. Xing, L. N. Quan, F. P. G. De Arquer, X. Gong, J. Lu, L. Xie, W. Zhao, D. Zhang, C. Yan, W. Li, X. Liu, Y. Lu, J. Kirman, E. H. Sargent, Q. Xiong, Z. Wei, *Nature* **2018**, *562*, 245.
[3] B. Guo, R. Lai, S. Jiang, L. Zhou, Z. Ren, Y. Lian, P. Li, X. Cao, S. Xing, Y. Wang, W. Li, C. Zou, M. Chen, Z. Hong, C. Li, B. Zhao, D. Di, *Nat. Photonics* **2022**, *16*, 637.
[4] M. I. Saidaminov, V. Adinolfi, R. Comin, A. L. Abdelhady, W. Peng, I. Dursun, M. Yuan, S. Hoogland, E. H. Sargent, O. M. Bakr, *Nat. Commun.* **2015**, *6*, 8724.
[5] M. I. Saidaminov, M. A. Haque, M. Savoie, A. L. Abdelhady, N. Cho, I. Dursun, U. Buttner, E. Alarousu, T. Wu, O. M. Bakr, *Adv. Mater.* **2016**, *28*, 8144.
[6] Y. Guan, C. Zhang, Z. Liu, Y. Zhao, A. Ren, J. Liang, F. Hu, Y. S. Zhao, *Adv. Mater.* **2022**, *34*, 2203201.
[7] H. Min, D. Y. Lee, J. Kim, G. Kim, K. S. Lee, J. Kim, M. J. Paik, Y. K. Kim, K. S. Kim, M. G. Kim, T. J. Shin, S. Il Seok, *Nature* **2021**, *598*, 444.
[8] J. J. Yoo, G. Seo, M. R. Chua, T. G. Park, Y. Lu, F. Rotermund, Y.-K. Kim, C. S. Moon, N. J. Jeon, J.-P. Correa-Baena, V. Bulovic, S. S. Shin, M. G. Bawendi, J. Seo, *Nature* **2021**, *590*, 587.
[9] R. Lin, J. Xu, M. Wei, Y. Wang, Z. Qin, Z. Liu, J. Wu, K. Xiao, B. Chen, S. M. Park, G. Chen, H. R. Atapattu, K. R. Graham, J. Xu, J. Zhu, L. Li, C. Zhang, E. H. Sargent, H. Tan, *Nature* **2022**, *603*, 73.
[10] S. D. Stranks, H. J. Snaith, *Nat. Nanotechnol.* **2015**, *10*, 391.
[11] B. R. Sutherland, E. H. Sargent, *Nat. Photonics* **2016**, *10*, 295.
[12] Y. Fu, H. Zhu, J. Chen, M. P. Hautzinger, X.-Y. Zhu, S. Jin, *Nat. Rev. Mater.* **2019**, *4*, 169.
[13] H. Zhu, Y. Fu, F. Meng, X. Wu, Z. Gong, Q. Ding, M. V. Gustafsson, M. T. Trinh, S. Jin, X.-Y. Zhu, *Nat. Mater.* **2015**, *14*, 636.
[14] Y. Jia, R. A. Kerner, A. J. Grede, B. P. Rand, N. C. Giebink, *Nat. Photonics* **2017**, *11*, 784.
[15] C. Huang, C. Zhang, S. Xiao, Y. Wang, Y. Fan, Y. Liu, N. Zhang, G. Qu, H. Ji, J. Han, L. Ge, Y. Kivshar, Q. Song, *Science* **2020**, *367*, 1018.
[16] S. W. Eaton, M. Lai, N. A. Gibson, A. B. Wong, L. Dou, J. Ma, L.-W. Wang, S. R. Leone, P. Yang, *Proc. Natl. Acad. Sci. U. S. A.* **2016**, *113*, 1993.
[17] Y. Fu, H. Zhu, C. C. Stoumpos, Q. Ding, J. Wang, M. G. Kanatzidis, X. Zhu, S. Jin, *ACS Nano* **2016**, *10*, 7963.
[18] Q. Zhang, R. Su, X. Liu, J. Xing, T. C. Sum, Q. Xiong, *Adv. Funct. Mater.* **2016**, *26*, 6238.

[19] N. G. Horton, K. Wang, D. Kobat, C. G. Clark, F. W. Wise, C. B. Schaffer, C. Xu, *Nat. Photonics* **2013**, *7*, 205.
[20] J. Wu, Y. Liang, S. Chen, C.-L. Hsu, M. Chavarha, S. W. Evans, D. Shi, M. Z. Lin, K. K. Tsia, N. Ji, *Nat. Methods* **2020**, *17*, 287.
[21] C.-C. Liu, H.-H. Hsiao, Y.-C. Chang, *Sci. Adv.* **2023**, *9*, eadf6649.
[22] S. Li, D. Lei, W. Ren, X. Guo, S. Wu, Y. Zhu, A. L. Rogach, M. Chhowalla, A. K.-Y. Jen, *Nat. Commun.* **2020**, *11*, 1192.
[23] J. E. Ehrlich, X. L. Wu, I.-Y. S. Lee, Z.-Y. Hu, H. Röckel, S. R. Marder, J. W. Perry, *Opt. Lett.* **1997**, *22*, 1843.
[24] Y. Wang, X. Li, X. Zhao, L. Xiao, H. Zeng, H. Sun, *Nano Lett.* **2016**, *16*, 448.
[25] Y. He, R. Su, Y. Huang, Y. Zhou, Q. Zhao, J. B. Khurgin, Q. Xiong, X. Xu, *Adv. Funct. Mater.* **2019**, *29*, 1904694.
[26] Z. Shi, F. Zhang, J. Yan, Y. Zhang, X. Chen, S. Chen, D. Wu, X. Li, Y. Zhang, C. Shan, *Nano Res.* **2022**, *15*, 492.
[27] Y. Xu, Q. Chen, C. Zhang, R. Wang, H. Wu, X. Zhang, G. Xing, W. W. Yu, X. Wang, Y. Zhang, M. Xiao, *J. Am. Chem. Soc.* **2016**, *138*, 3761.
[28] M. J. Crane, L. M. Jacoby, T. A. Cohen, Y. Huang, C. K. Luscombe, D. R. Gamelin, *Nano Lett.* **2020**, *20*, 8626.
[29] S. Yu, J. Xu, X. Shang, E. Ma, F. Lin, W. Zheng, D. Tu, R. Li, X. Chen, *Adv. Sci.* **2021**, *8*, 2100084.
[30] D. Niesner, O. Schuster, M. Wilhelm, I. Levchuk, A. Osvet, S. Shrestha, M. Batentschuk, C. Brabec, T. Fauster, *Phys. Rev. B* **2017**, *95*, 075207.
[31] Z. Liu, Q. Shang, C. Li, L. Zhao, Y. Gao, Q. Li, J. Chen, S. Zhang, X. Liu, Y. Fu, Q. Zhang, *Appl. Phys. Lett.* **2019**, *114*, 101902.
[32] A. Shinde, R. Gahlaut, S. Mahamuni, *J. Phys. Chem. C* **2017**, *121*, 14872.
[33] X. Lao, Z. Yang, Z. Su, Y. Bao, J. Zhang, X. Wang, X. Cui, M. Wang, X. Yao, S. Xu, *J. Phys. Chem. C* **2019**, *123*, 5128.
[34] Y. Liu, J. Xu, R. Jia, L. Song, J. Lu, J. Dai, *J. Mater. Chem. C* **2022**, *10*, 16679.
[35] Q. Zhang, S. T. Ha, X. Liu, T. C. Sum, Q. Xiong, *Nano Lett.* **2014**, *14*, 5995.
[36] J. Lu, C. Zhang, F. Li, R. Wang, F. Qin, G. Zhu, *Appl. Phys. Lett.* **2022**, *120*, 171105.
[37] B. Tang, H. Dong, L. Sun, W. Zheng, Q. Wang, F. Sun, X. Jiang, A. Pan, L. Zhang, *ACS Nano* **2017**, *11*, 10681.
[38] Z. Yang, J. Lu, M. Zhuge, Y. Cheng, J. Hu, F. Li, S. Qiao, Y. Zhang, G. Hu, Q. Yang, D. Peng, K. Liu, C. Pan, *Adv. Mater.* **2019**, *31*, 1900647.
[39] F. Li, Z. Yang, M. Jiang, C. Wang, J. Xi, Y. Zhang, C. Pan, J. Lu, R. Wang, *Appl. Phys. Lett.* **2021**, *118*, 071103.